J|A|C|S
ARTICLES
Published on Web 01/27/2004

Definitive Spectroscopic Determination of Zero-Field Splitting in High-Spin Cobalt(II)

J. Krzystek,*,† S. A. Zvyagin,† Andrew Ozarowski,† Adam T. Fiedler,‡ Thomas C. Brunold,‡ and Joshua Telser§

Contribution from the National High Magnetic Field Laboratory, Florida State University, Tallahassee, Florida 32310, Department of Chemistry, University of Wisconsin, Madison, Wisconsin 53706, and Chemistry Program, Roosevelt University, Chicago, Illinois 60605

Received October 27, 2003; E-mail: krzystek@magnet.fsu.edu

Abstract: A high-spin Co(II) complex ($3d^7$, $S = 3/2$), $Co(PPh_3)_2Cl_2$ (Ph = phenyl), has been investigated in the solid state by both high-frequency and -field electron paramagnetic resonance (HFEPR) and by variable-temperature, variable-field magnetic circular dichroism (VTVH-MCD). In HFEPR spectroscopy, the combination of variable sub-THz frequencies generated by backward wave oscillators (150−700 GHz, corresponding to energy 5−23 cm^{-1}) and high magnetic fields (0−25 T) constitutes a novel experimental technique allowing accurate determination of a complete set of spin Hamiltonian parameters for this complex: $D = -14.76(2)$ cm^{-1}, $E = 1.141(8)$ cm^{-1}, $g_x = 2.166(4)$, $g_y = 2.170(4)$, $g_z = 2.240(5)$. Independent VTVH-MCD studies on multiple absorption bands of the complex yield $D = -14(3)$ cm^{-1}, $E = 0.96(20)$ cm^{-1} ($|E/D| = 0.08(2)$), $g_x = 2.15(5)$, $g_y = 2.16(4)$, and $g_z = 2.17(3)$. This very good agreement between HFEPR and MCD indicates that there is no inherent discrepancy between these two quite different experimental techniques. Thus, depending on the nature of the sample, either can be reliably used to determine zero-field splitting parameters in high-spin Co(II), with the HFEPR being more accurate but VTVH-MCD being more sensitive.

Introduction

The cobalt(II) ion has attracted considerable attention because of its ability to replace zinc in a variety of enzymes,[1−7] without significantly affecting their activity. Closed-shell (d^{10}) Zn(II) cannot be investigated by most spectroscopic techniques, but the situation is very different for Co(II) (d^7), which is amenable to multiple methods.[1,3−5,7,8] Most biological Zn sites are four-coordinate, and thus substitution for Zn(II) leads to Co(II) in a high-spin ground state ($S = 3/2$). In this case, an important experimental parameter is the zero-field splitting (zfs),[9] i.e., the energy difference between the two Kramers doublets, $|S, M_S\rangle = |3/2, \pm1/2\rangle$ and $|3/2, \pm3/2\rangle$.[10] The zfs arises under conditions of lower than cubic symmetry.[11] However, in most Co(II) complexes the zfs cannot be measured by the most direct method, i.e., conventional EPR, since the splitting energy usually greatly exceeds the microwave quantum energy (typically 0.3 cm^{-1} for X-band EPR). Instead, the zfs has been indirectly deduced from the CW power saturation behavior of EPR signals,[4,12,13] from the effective g values (g'),[3,14] or from nonresonant methods: magnetic susceptibility/magnetization/specific heat studies[15−17] and most notably VT-MCD.[5,18] An extensive comparison of these techniques has been made,[18] which raised the issue whether, given the existing discrepancies among the results obtained from them, all mentioned techniques actually measure the same parameter. Obviously, a conclusive measurement of zfs is very desirable, since this parameter—

† Florida State University.
‡ University of Wisconsin.
§ Roosevelt University.

(1) Maret, W.; Vallee, B. L. *Methods Enzymol.* **1993**, *226*, 52−65.
(2) Bencini, A.; Bertini, I.; Canti, G.; Gatteschi, D.; Luchinat, C. *J. Inorg. Biochem.* **1981**, *14*, 81−93.
(3) Banci, L.; Bencini, A.; Benelli, C.; Gatteschi, D.; Zanchini, C. *Struct. Bonding* **1982**, *52*, 37−86.
(4) Kuo, L. C.; Makinen, M. W. *J. Am. Chem. Soc.* **1985**, *107*, 5255−5261.
(5) Werth, M. T.; Tang, S.-F.; Formicka, G.; Zeppezauer, M.; Johnson, M. K. *Inorg. Chem.* **1995**, *34*, 218−228.
(6) Adrait, A.; Jacquamet, L.; Le Pape, L.; Gonzalez de Peredo, A.; Aberdam, D.; Hazemann, J.-L.; Latour, J.-M.; Michaud-Soret, I. *Biochemistry* **1999**, *38*, 6248−6260.
(7) Walsby, C. J.; Krepkiy, D.; Petering, D. H.; Hoffman, B. M. *J. Am. Chem. Soc.* **2003**, *125*, 7502−7503.
(8) Bencini, A.; Benelli, C.; Gatteschi, D.; Zanchini, C. *Inorg. Chem.* **1979**, *18*, 2137−2140.
(9) Abbreviations used: CW, continuous wave; EPR, electron paramagnetic resonance; HFEPR, high-frequency and -field EPR; MCD, magnetic circular dichroism; VTVH-MCD, variable temperature−variable field MCD; zfs, zero-field splitting.
(10) For clarity, we will use only the M_S number to denote the two Kramers doublets, i.e., $\pm1/2$ and $\pm3/2$ throughout, noting that these are not "good" quantum numbers in all cases.
(11) Zfs is often represented by the symbol Δ, which in the case of $S = 3/2$ is equal to $2(D^2 + 3E^2)^{1/2}$, where D and E are parameters in the spin Hamiltonian (1).
(12) Makinen, M. W.; Yim, M. B. *Proc. Natl. Acad. Sci. U.S.A.* **1981**, *78*, 6221−6225.
(13) Makinen, M. W.; Kuo, L. C.; Yim, M. B.; Wells, G. B.; Fukuyama, J. M.; Kim, J. E. *J. Am. Chem. Soc.* **1985**, *107*, 5245−5255.
(14) McGarvey, B. R. In *Transition Metal Chemistry*; Carlin, R. L., Ed.; Marcel Dekker: New York, 1966; pp 89−201.
(15) Duggan, D. M.; Hendrickson, D. N. *Inorg. Chem.* **1975**, *14*, 1944−1956.
(16) Carlin, R. L.; Chirico, R. D.; Sinn, E.; Mennenga, G.; De Jongh, L. J. *Inorg. Chem.* **1982**, *21*, 2218−2222.
(17) Rizzi, A. C.; Brondino, C. D.; Calvo, R.; Baggio, R.; Garland, M. T.; Rapp, R. E. *Inorg. Chem.* **2003**, *42*, 4409−4416.
(18) Larrabee, J. A.; Alessi, C. M.; Asiedu, E. T.; Cook, J. O.; Hoerning, K. R.; Klingler, L. J.; Okin, G. S.; Santee, S. G.; Volkert, T. L. *J. Am. Chem. Soc.* **1997**, *119*, 4182−4196.

10.1021/ja039257y CCC: $27.50

Chart 1. Structure of $CoCl_2(PPh_3)_2$

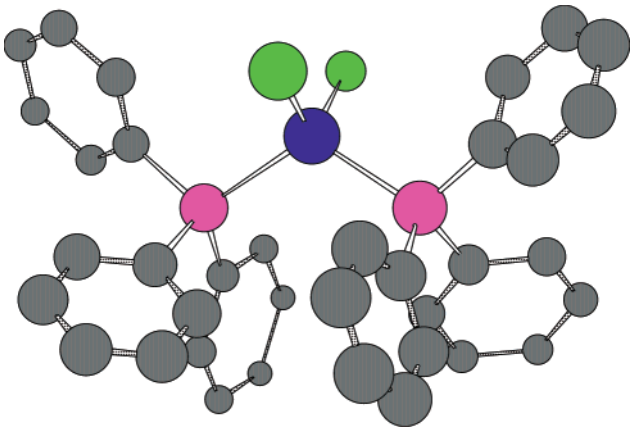

analyzed within the framework of ligand field theory calculations[18,19]—is of great importance in determining the electronic and, in ideal cases, geometric structure of Co(II) in a model compound or in an enzyme active site.[3,13,18]

A rare example of the direct measurement of zfs in high-spin Co(II) is an early HFEPR study on single crystals of Cs_3CoX_5 (X = Cl, Br) by van Stapele et al.[20] These workers employed pulsed magnetic fields up to 9 T and frequencies of 90 and 120 GHz to accurately measure relatively large zfs ($D = -4.30$ (X = Cl), -5.34 cm^{-1} (X = Br)).[20] We describe here the use of HFEPR to study another pseudo-tetrahedral (C_{2v} symmetry) Co(II) complex, $CoCl_2(PPh_3)_2$ (Ph = phenyl; the structure is shown in Chart 1, based on Carlin et al.[16]), but with a novel methodology and a vastly extended range of sub-THz frequencies (up to 700 GHz) combined with swept high fields (up to 25 T) generated by a Bitter-type resistive magnet. Our HFEPR methods allow a precise determination of large magnitude zfs ($|\Delta| \approx 30$ cm^{-1}) in $CoCl_2(PPh_3)_2$. This complex was not among the many described in the MCD study by Larrabee et al.[18] but was studied by Makinen et al.[13] using X-band EPR and by EPR saturation methods to determine the zfs. Because there exists controversy among the various experimental techniques employed for this measurement, particularly between EPR and MCD,[18] we have concurrently applied VTVH-MCD for the measurement of zfs in $CoCl_2(PPh_3)_2$, with the aim of comparing the results obtained independently by both techniques. It should be noted that given the current state-of-the-art of HFEPR, its concentration sensitivity may not be sufficient to study actual enzymes in aqueous solutions; however, it is perfectly suitable to studying model complexes such as $CoCl_2(PPh_3)_2$. In this respect, HFEPR and MCD can be complementary, since the latter, being an optical technique, is inherently more sensitive than the former.

Experimental Section

Samples. $CoCl_2(PPh_3)_2$ was obtained from Sigma-Aldrich or prepared by the method of Venzani.[21] For HFEPR, the material was used in two forms: (a) loose polycrystalline material and (b) sample ground with an agate mortar and pestle and pressed into a KBr pellet (2:1 by weight KBr:$CoCl_2(PPh_3)_2$) to constrain the crystallites and improve optical transparency at sub-THz frequencies. For MCD, the sample was ground in a glovebox. Poly(dimethylsiloxane) was added to the powder and thoroughly mixed to obtain a mull. A small amount of this mull was then suspended between two quartz disks that were mounted in an MCD sample cell in a nitrogen atmosphere. The sample cell was immediately frozen in liquid nitrogen upon removal from the glovebox.

HFEPR Instrumentation. HFEPR measurements were made using the new sub-THz spectroscopy facility at NHMFL.[22] The tunable frequencies in the 150−700 GHz range (~5−23 cm^{-1} energy) were provided by a set of four backward wave oscillators (Institute of General Physics, Moscow, Russian Federation). The high-voltage power supply and the permanent magnet housing for the tubes were acquired from the same source. The frequency was precalibrated using a Fabry−Perot interferometer. The magnet used was the 25 T resistive Bitter-type "Keck" magnet of improved homogeneity (12 ppm in 1 cm diameter) and temporal stability. The field was precalibrated using an NMR probe and was checked during the experiment using a DPPH marker. The oversized-pipe wave propagation system was home-built along the principles outlined before.[23] No resonator was used. Detection was provided with an InSb hot-electron bolometer (QMC Ltd., Cardiff, U.K.). Modulation for detection purposes was provided alternatively by modulating the magnetic field (1 kHz frequency, 1 mT max. amplitude) or by chopping the sub-THz beam at ca. 300 Hz. A Stanford SR830 lock-in amplifier converted the modulated signal to DC voltage.

HFEPR Analysis. The magnetic properties of an ion with $S = 3/2$ can be described by the standard spin Hamiltonian comprised of Zeeman and zfs terms[24]

$$H = \beta B \cdot \mathbf{g} \cdot S + D(S_z^2 - S(S+1)/3) + E(S_x^2 - S_y^2) \qquad (1)$$

The EPR resonances were collected as a function of sub-THz quantum energy, and the resulting 2-dimensional (field vs energy) array was simultaneously fitted by use of a nonlinear least-squares (Simplex) method to minimize the function

$$\chi^2 = \sum_{i=1}^{N} (f_i^{(calc)} - f_i^{(exp)})^2 \qquad (2)$$

where f_i are the calculated and experimental resonance fields. The resonance fields were calculated in an iterative procedure that employed the Householder method[25] to diagonalize the spin Hamiltonian in eq 1. This least-squares procedure was used in conjunction with human judgment, which served to eliminate mathematically possible, but unphysical, results to obtain best-fit parameters for the entire field vs energy array of EPR transitions. Errors in the parameters were estimated by use of the Hessian matrix method.[26] The transition probabilities were calculated from the eigenvectors in a standard way.[27] The calculated transition intensities were corrected for the Boltzmann populations of the levels involved. This correction was necessary since the zfs and Zeeman energies were much higher than kT at the low temperatures at which HFEPR spectra were recorded.

MCD Instrumentation and Analysis. MCD spectra were measured using a Jasco J-715 spectropolarimeter in conjunction with an Oxford Instruments SM-4000 8T magnetocryostat. VTVH-MCD data were fit using the software developed by Dr. Frank Neese (MPI Mülheim, Germany).[28]

(19) Horrocks, W. D.; Burlone, D. A. *J. Am. Chem. Soc.* **1976**, *98*, 6512−6516.
(20) van Stapele, R. P.; Beljers, H. G.; Bongers, P. F.; Zijlstra, H. *J. Chem. Phys.* **1966**, *44*, 3719−3725.
(21) Venzani, L. M. *J. Chem. Soc.* **1958**, 719−724.
(22) Zvyagin, S. A.; Krzystek, J.; van Loosdrecht, P. H. M.; Dhalenne, G.; Revcolevschi, A. *Phys. Rev. B* **2003**, *67*, 212403.
(23) Hassan, A. K.; Pardi, L. A.; Krzystek, J.; Sienkiewicz, A.; Goy, P.; Rohrer, M.; Brunel, L.-C. *J. Magn. Reson.* **2000**, *142*, 300−312.
(24) Abragam, A.; Bleaney, B. *Electron Paramagnetic Resonance of Transition Ions*; Dover Publications: New York, 1986.
(25) Wilkinson, J. H. *The Algebraic Eigenvalue Problem*; Clarendon Press: London, 1970.
(26) Press, W. H.; Flannery, B. P.; Teukolsky, A. A.; Vetterling, W. T. In *Numerical Recipes in Pascal*; Cambridge University Press: Cambridge, 1989, p 572.
(27) Bencini, A.; Gatteschi, D. In *Transition Metal Chemistry*; Melson, G. A., Figgis, B. N., Eds.; Marcel Dekker: New York, 1982; Vol. 8, p 1.
(28) Neese, F.; Solomon, E. I. *Inorg. Chem.* **1999**, *38*, 1847−1865.

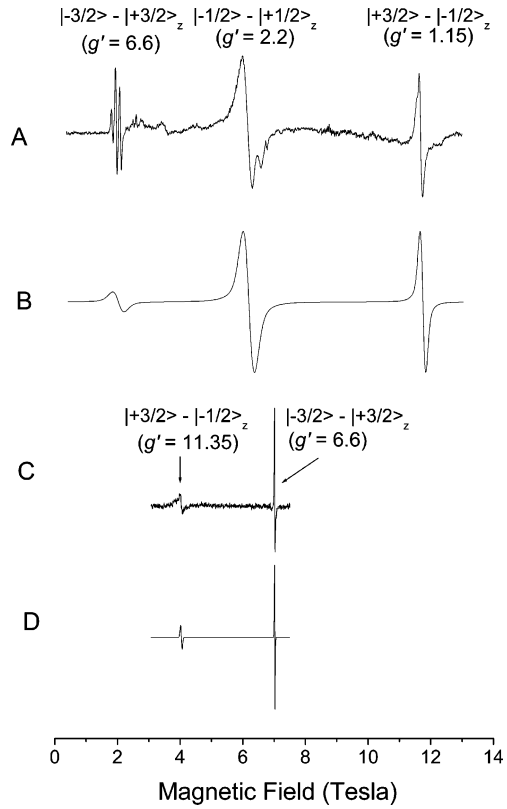

Figure 1. HFEPR spectra of loose polycrystalline $CoCl_2(PPh_3)_2$. (A) Experiment at 190 GHz and 20 K; (B) Simulation at 190 GHz and 20 K; (C) Experiment at 643 GHz and 4.7 K; (D) Simulation at 643 GHz and 4.7 K. Simulations assumed a field-induced orientation of the crystallites along the zfs axis *z*, B_1 both parallel and perpendicular to B_0, and used the following spin Hamiltonian parameters: $D = -14.76$ cm^{-1}, $E = 1.141$ cm^{-1}, $g_x = 2.166$, $g_y = 2.170$, $g_z = 2.240$ (B), and $D = -14.66$ cm^{-1}, $E = 1.141$ cm^{-1}, $g_x = 2.166$, $g_y = 2.170$, $g_z = 2.197$ (D). Particular transitions were identified using plots in Figure 4 and labeled accordingly.

Results

HFEPR Spectroscopy of $CoCl_2(PPh_3)_2$. As seen in Figure 1, an HFEPR spectrum of *loose*, polycrystalline solid $CoCl_2(PPh_3)_2$ at low temperatures (2−5 K) typically comprises two features: a tightly spaced group of signals found for all fields and frequencies at an effective *g* value, $g' \approx 6.6$, and a single peak which appears at a different g' value for each frequency, e.g., at $g' = 1.15$ at 190 GHz (Figure 1A) and $g' = 11.35$ at 643 GHz (Figure 1C). At elevated temperatures (>10 K with a maximum at ca. 37 K), another signal appears that is characterized by $g' \approx 2.2$ at low fields (Figure 1A). The form of the $g' \approx 6.6$ group of lines is not fully reproducible, as both their number and intensities vary from sample to sample. At high enough frequencies and, correspondingly, magnetic fields, the spectrum becomes simplified and the $g' \approx 6.6$ group collapses to a single line (Figure 1C). It should be noted that while the $g' \approx 6.6$ line(s) move to higher fields with increasing frequency, the reverse is true for the peak visible at 11.7 T at 190 GHz and 4.05 T at 643 GHz. In Figure 1B and 1D we also offer spectra simulated using spin Hamiltonian parameters best-fitted for the given frequency. As is often the case in high-spin systems (see, e.g., Figure 6 in Mantel et al.[29]), it is difficult using this method to produce a unique set of parameters reproducing equally well spectra at all frequencies; thus the final and most accurate values were obtained using a different tunable-frequency methodology (see below). To obtain good agreement between simulation and experiment in Figure 1 we had to assume that at a given frequency (i) all the crystallites were oriented with their largest zfs principal axis (*z*) along the field due to a strong magnetic torquing effect and (ii) the sample was exposed to oscillating B_1 field components that are both perpendicular *and* parallel to the Zeeman (B_0) field.[30] We were unable to simulate the exact appearance of the $g' \approx 6.6$ signal at low frequencies/fields. The fact that its appearance is not fully reproducible and field-dependent strongly suggests the presence of artifacts that often accompany magnetic torquing. We have previously observed similar artifacts in several polycrystalline high-spin transition-metal complexes such as porphyrinic complexes of Mn(III)[31] or pseudo-tetrahedral complexes of Ni(II), the latter including the same ligands as in this work (PPh_3 and Cl).[32] The spectra presented in Figure 1 can be thus called "quasi-single crystal spectra", with the term "quasi" meaning that the crystallites do not become ideally oriented in field (as achievable in a true single-crystal study) but predominantly choose discrete orientations very close to $B_0 \parallel z$. The torquing is not complete, as weak signals are observed that can be well simulated using a powder pattern orientation with the spin Hamiltonian parameters derived below.

Since the spectra obtained for one particular orientation of the complex relative to the magnetic field do not usually allow one to determine all the relevant parameters of the spin Hamiltonian and to confirm the presence of magnetic torquing, we proceeded to immobilize the crystallites by pressing the powder into a pellet. To increase the optical translucency of the pellet in the sub-THz frequencies region, we mixed the sample with KBr prior to pressing the pellet, similarly to what is often done in infrared spectroscopy. This usually increased the signal-to-noise ratio and generally improved the spectral quality.

A low-temperature (2.0 K) spectrum of such a *pellet*, shown in Figure 2A, consists of two lines appearing in the 13−25 T field range for frequencies in the 150−240 GHz range. These signals are actually very strong, with the 15.8 T line representing a ca. 30% reduction of the incident mm wave power transmitted through the sample. However, they are also very broad, with the peak-to-peak line width, ΔB_{pp}, on the order of 0.7 T for the same line. This makes the usual method of magnetic field modulation, with its limited amplitude, extremely inefficient and is the reason for the moderate signal-to-noise ratio of the spectra presented in Figure 2. A much better signal-to-noise ratio was obtained with modulation of the sub-THz beam using a chopper (optical modulation);[33] however, such spectra usually suffer from baseline instability problems.

At high temperatures (above 10 K, with the maximum at about 37 K), another pair of lines appears at lower fields (in the $g' \approx 3.65-4.9$ range in Figure 2C) while the signals

(29) Mantel, C.; Hassan, A. K.; Pécaut, J.; Deronzier, A.; Collomb, M.-N.; Duboc-Toia, C. *J. Am. Chem. Soc.* **2003**, *125*, 12337−12344.

(30) This phenomenon can be attributed to multiple reflections and general imperfections (mode impurity) of the sub-THz propagation system employing no resonator.

(31) Krzystek, J.; Telser, J.; Pardi, L. A.; Goldberg, D. P.; Hoffman, B. M.; Brunel, L.-C. *Inorg. Chem.* **1999**, *38*, 6121−6129.

(32) Krzystek, J.; Park, J.-H.; Meisel, M. W.; Hitchman, M. A.; Stratemeier, H.; Brunel, L.-C.; Telser, J. *Inorg. Chem.* **2002**, *41*, 4478−4487.

(33) Krzystek, J.; Zvyagin, S. A.; Ozarowski, A.; Telser, J. To be submitted to *J. Magn. Reson.*

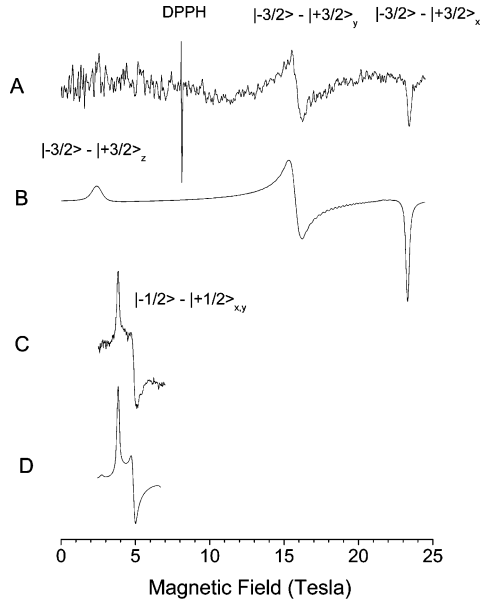

Figure 2. HFEPR spectra of a $CoCl_2(PPh_3)_2$ pellet. (A) Experiment at 225 GHz and 2.0 K; (B) Simulation at 225 GHz and 2.0 K; (C) Experiment at 256 GHz and 37 K; (D) Simulation at 256 GHz and 37 K. Simulations assumed a powder pattern and used the same set of spin Hamiltonian parameters as Figure 1B. Particular transitions were identified using plots in Figure 4 and labeled accordingly.

described in the previous paragraph lose intensity and disappear in the noise. Both the low- and high-temperature spectra can be nicely reproduced by simulations (Figure 2B and 2D), using the same set of spin Hamiltonian parameters, if we assume that a true powder distribution of the complex is obtained in the pellet, thus confirming the magnetic torquing effect in the loose powder. (The parallel line within the $M_S = \pm 3/2$ Kramers doublet, visible in the simulation in Figure 2B, is buried in the noise in Figure 2A.) The low-temperature lines originating from the $\pm 3/2$ Kramers doublet are visibly broader (line widths up to 0.7 T) than their high-temperature counterparts originating from the $\pm 1/2$ Kramers doublet (line widths of 0.1−0.2 T). Considering that the former appear at much higher fields than the latter, a plausible reason for the broader line widths of the $\pm 3/2$ Kramers doublet transitions is the *D*-strain effect that often appears in HFEPR spectra.

To facilitate the interpretation of the observed spectra, we provide in Figure 3 energy-level diagrams generated for the three canonical field orientations using the spin Hamiltonian parameters determined below. One can see that for an $S = 3/2$ system with a rhombic distortion ($E \neq 0$), the field vs energy dependencies are quite complicated due to level mixing and anti-crossing, which results in the effective *g*'s varying strongly with field for most of the transitions. In Figure 3 we also indicate by arrows the specific experimental resonances observed in Figures 1 and 2.

To interpret the HFEPR spectra and to extract accurate spin-Hamiltonian parameter values from them, we performed a tunable-frequency experiment, varying the sub-THz frequency over the entire range available, ca. 150−700 GHz. We plot the obtained results in Figure 4 as a dependence of the resonances on the sub-THz quantum energy at which they are observed. The squares represent the lines observable in a loose (field-oriented) sample, while the triangles represent the resonances observed in a pellet. In the case of the $g' \approx 6.6$ signal observed

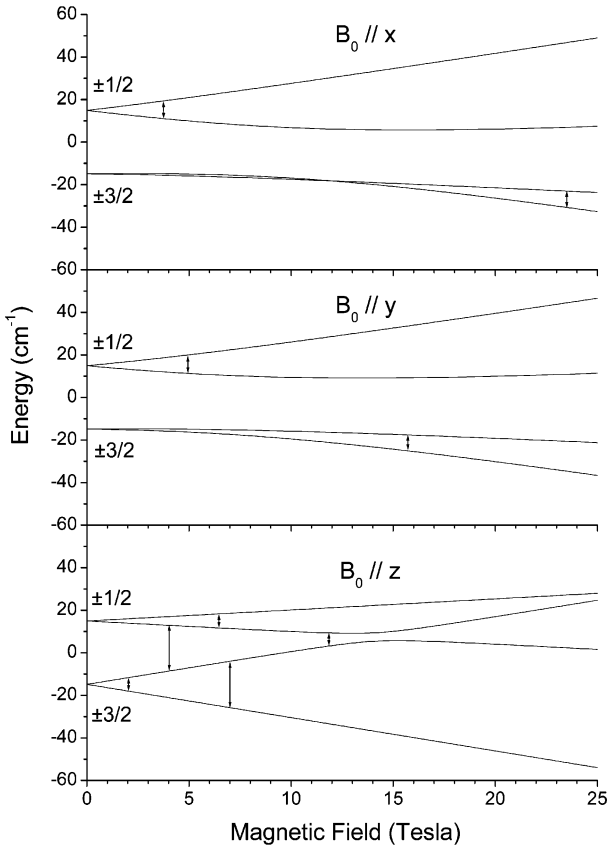

Figure 3. Energy levels as a function of magnetic field for the three canonical orientations of the field relative to the principal zfs axis calculated for $CoCl_2(PPh_3)_2$ using the spin Hamiltonian parameters given in Figure 1. EPR transitions observed in a field-oriented sample and shown in Figure 1 are marked with arrows for $B_0 \parallel z$ (short arrows, 190 GHz; long arrows, 643 GHz). Transitions observed in a pellet and shown in Figure 2 are marked with arrows (225 and 256 GHz are indistinguishable) and shown for $B_0 \parallel x$ and $B_0 \parallel y$.

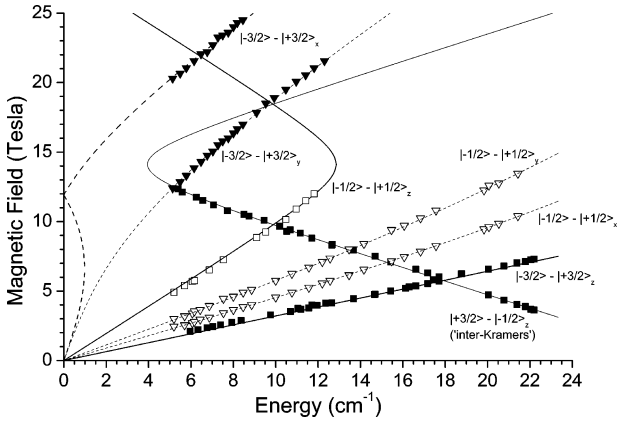

Figure 4. Resonance field vs sub-THz quantum energy dependence for EPR transitions in $CoCl_2(PPh_3)_2$. Experimental points for the loose sample are represented by squares and those for the pellet by triangles. Full symbols represent data at low temperatures (2.0−4.7 K); empty symbols are for data at high temperatures (20−37 K). Simulations using the following spin Hamiltonian parameters obtained from a least-squares fit to the experimental resonances, $S = 3/2$, $D = -14.76$ cm^{-1}, $E = 1.141$ cm^{-1}, $g_x = 2.166$, $g_y = 2.170$, $g_z = 2.240$, are shown by solid lines for parallel transitions and dashed lines for perpendicular transitions. Particular transition branches are identified and labeled accordingly.

in a loose sample, the position of the lowest-field signal was used if artifacts occurred in that specific case. We also differentiate between the low-temperature signals, represented

by filled symbols, and the high-temperature resonances, represented by empty symbols.

The observed resonances form two different kinds of transition branches: those that extrapolate to zero field at zero energy and a single branch that goes against the trend, i.e., decreases in field with increasing energy and extrapolates to zero field at a finite energy value of about 30 cm^{-1}. Comparison with Figure 3 quickly shows that the latter must be an *inter*-Kramers transition, i.e., one taking place *between* the $\pm 1/2$ and $\pm 3/2$ Kramers doublets, and since it appears in the field-torqued sample, it is the parallel turning point ($B_0 \parallel z$) of that particular transition. Also, following Figure 3, we may see that the 30 cm^{-1} intercept represents the zero-field energy gap between these two Kramers doublets; this value is thus the zfs (Δ). The inter-Kramers transition is therefore the most informative with regard to a direct evaluation of the zfs. In our spectra, we only see the parallel turning point of that transition, since the perpendicular resonances ($B_0 \parallel x,y$) appear at frequencies much higher than the range available to us. In the absence of torquing, the intensity of the parallel turning point is much reduced, but even in such a case, simulations show that it is possible to obtain all the relevant spin Hamiltonian parameters from the remaining (intra-Kramers) transitions, albeit with reduced accuracy.[34] Thus, although we were greatly assisted by magnetic torquing, HFEPR is a suitable technique also in the absence of this effect.

To refine the zfs value and obtain a complete set of spin Hamiltonian parameters, we performed a new simulation procedure that fits those parameters simultaneously to the complete set of resonances as arranged in a 2-dimensional (field vs energy) array and shown in Figure 4. We underscore here the fact that we did not use single-frequency simulations for this purpose since quite often in high-spin systems such as $S = 3/2$, good agreement at one frequency does not guarantee success at another.[35] In simulating the resonances we achieved a much greater precision, arriving at the following best-fit values: $D = -14.76(2)$ cm^{-1}, $E = 1.141(8)$ cm^{-1}, $g_x = 2.166(4)$, $g_y = 2.170(4)$, $g_z = 2.240(5)$.[36] This set of spin Hamiltonian parameters was subsequently used to calculate the expected dependencies of the resonances on the sub-THz quantum energy. The calculations are presented as curves in Figure 4. The simulated curves show excellent agreement with the experimental points and allowed us to unequivocally attribute observed resonances to particular turning points. We were thus able to label accordingly both the single-frequency spectra shown in Figures 1 and 2 and the field/energy dependencies in Figure 4. For comparative purposes, we calculate the zfs magnitude Δ of 29.76 cm^{-1}, using the formula $\Delta = 2(D^2 + 3E^2)^{1/2}$.

The temperature dependence of particular resonances allowed us in turn to determine the sign of the axial zfs parameter, D. Since the transitions within the $\pm 1/2$ Kramers doublet (empty symbols in Figure 4) do not appear at low temperatures but are detectable at elevated temperatures, this doublet is thermally activated and must lie higher in energy than the $\pm 3/2$ doublet, which is observable at low temperatures only. This situation, by convention, corresponds to a negative D value, which is thus unambiguously determined.

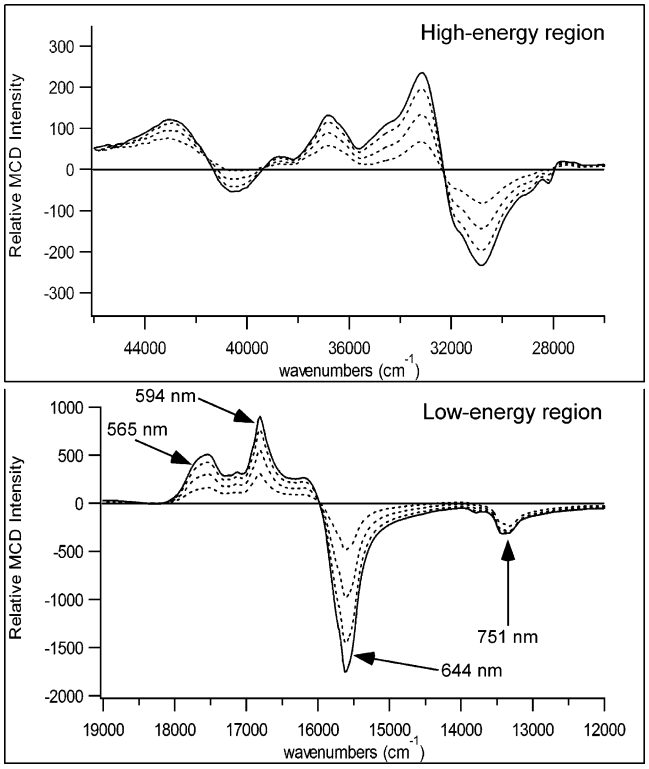

Figure 5. UV−visible variable-temperature MCD spectra for solid $CoCl_2(PPh_3)_2$ in the high-energy (top) and low-energy (bottom) regions. Spectra were recorded at a magnetic field of 7 T and at temperatures of 4, 8, 15, and 30 K. MCD intensities for all bands increase with decreasing temperature, characteristic of *C*-term behavior. The arrows indicate wavelengths at which VTVH-MCD data were collected.

Last, we note that no hyperfine coupling from ^{59}Co (100%, $I = 7/2$) was observed, and none was expected in these magnetically nondilute samples. However, no hyperfine coupling was observed by Makinen et al.[13] in the X-band EPR spectra at 3.6 K either, although they reported on the same complex in two magnetically dilute systems: polycrystalline $Co_{0.002}Zn_{0.998}Cl_2(PPh_3)_2$ and $CoCl_2(PPh_3)_2$ in ethanol frozen solution. Likewise, very broad EPR spectra with no resolved hyperfine coupling are generally observed for Co(II) complexes[37] and for Co(II)-substituted Zn proteins, such as carbonic anhydrase (at X-band),[2] a Zn-finger protein (at 35 GHz),[7] as well as for numerous other Zn proteins.[38]

MCD Spectroscopy of $CoCl_2(PPh_3)_2$. MCD spectra of $CoCl_2(PPh_3)_2$ obtained at low temperatures (4−30 K) are displayed in Figure 5. All band intensities are temperature-dependent, which is characteristic of *C*-term behavior as expected for this paramagnetic $S = 3/2$ spin system. The spectra display two sets of features—one set between 12 000 and 18 000 cm^{-1} and another set above 28 000 cm^{-1}. The low-energy bands are fairly weak in absorption ($\epsilon \approx 400$ $M^{-1}cm^{-1}$)[39] but very intense in MCD, permitting unambiguous assignment of these bands as ligand-field transitions.[40] As shown in previous

(34) In particular, the curving of the perpendicular resonances with increasing energy as in Figure 4 is a measure of D, while the splitting between them is a function of E.
(35) Krzystek, J.; Yeagle, G.; Park, J.-H.; Meisel, M. W.; Britt, R. D.; Brunel, L.-C.; Telser, J. *Inorg. Chem.* **2003**, *42*, 4610−4618.
(36) These are intrinsic g values in the $S = 3/2$ spin Hamiltonian (eq 1) not effective g' values in a fictitious $S' = 1/2$ spin Hamiltonian.
(37) Kang, P. C.; Eaton, G. R.; Eaton, S. S. *Inorg. Chem.* **1994**, *33*, 3660−3665.
(38) Walsby, C. J.; Hoffman, B. M. Personal communication of unpublished results.
(39) Simo, C.; Holt, S. *Inorg. Chem.* **1968**, *7*, 2655−2657.
(40) Johnson, M. K. In *Physical Methods in Bioinorganic Chemistry*; Que, L., Ed.; University Science Books: Sausalito, CA, 2000, pp 233−285.

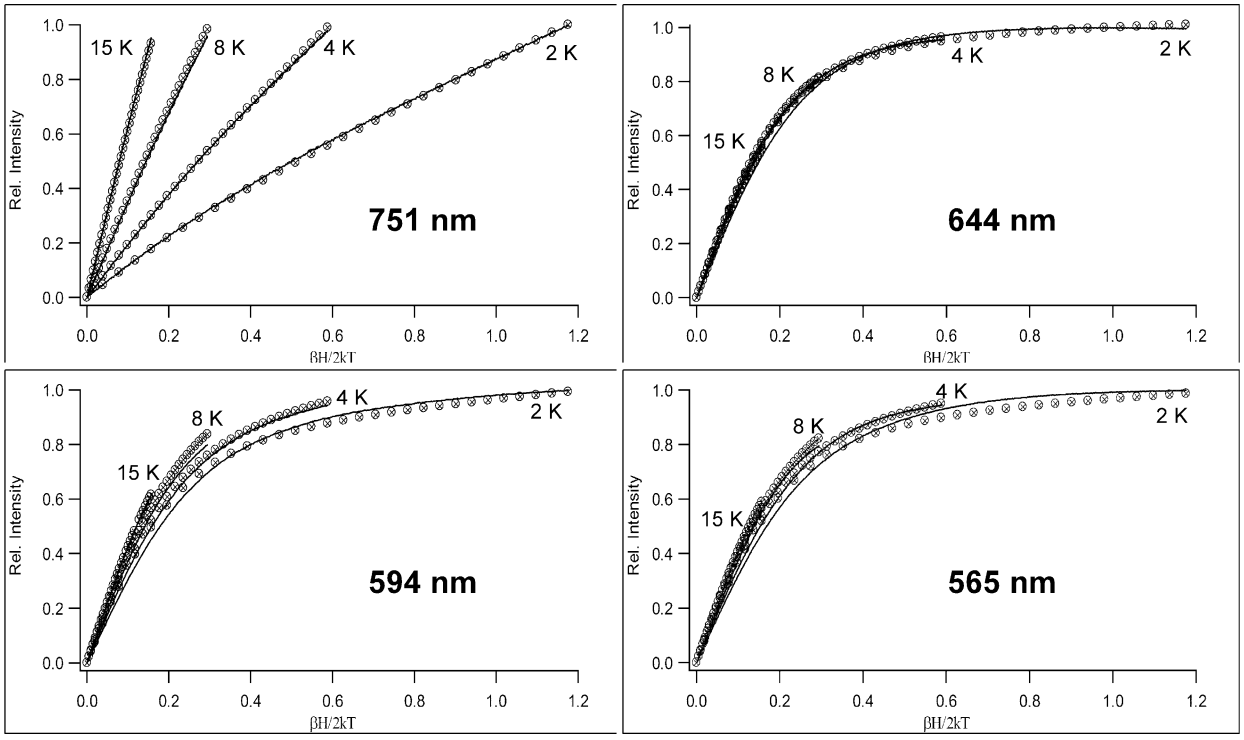

Figure 6. Experimental VTVH-MCD data at 751, 644, 594, and 565 nm for $CoCl_2(PPh_3)_2$ (solid lines). Data were obtained at 2, 4, 8, and 15 K with magnetic fields ranging from 0 to 7 T. Theoretical fits (⊗) were generated with the following spin-Hamiltonian parameters: $D = -12$ cm^{-1}, $E/D = 0.08$, $g_x = 2.1541$, $g_y = 2.1535$, and $g_z = 2.15$.

analyses of the absorption spectrum of $CoCl_2(PPh_3)_2$, these bands are components of the $^4A_2 \rightarrow {}^4T_1(P)$ transition in the parent T_d symmetry that is split by spin−orbit coupling and low-symmetry distortions.[39,41,42] The overall shape of the ligand-field region resembles previously published MCD spectra of high-spin, four-coordinate Co(II) complexes, consisting of a strong negative peak that is accompanied by negative features at low energy and a series of positive bands to higher energy.[18,43,44] The high-energy region is comprised of several bands that arise from charge-transfer (CT) transitions. This assignment is supported by the fact that these bands, while intense in the absorption spectrum, carry considerably less MCD intensity than the ligand-field transitions. Furthermore, when the chloride ligands are replaced with bromide ligands, yielding $CoBr_2(PPh_3)_2$, the high-energy bands red-shift by ~5000 cm^{-1}, indicating that these bands arise from halide-to-metal CT transitions (data not shown).

VTVH-MCD data for $CoCl_2(PPh_3)_2$ were collected at four wavelengths in the low-energy region: 751 nm (13 316 cm^{-1}), 644 nm (15 528 cm^{-1}), 594 nm (16 835 cm^{-1}), and 565 nm (17 699 cm^{-1}). These four wavelengths are indicated by the arrows in Figure 5 and were selected because they correspond to the peak positions of the four absorption bands observed for $CoCl_2(PPh_3)_2$ in the visible region.[39] In the VTVH-MCD experiments, the signal intensity at a particular wavelength was measured at four different temperatures (2, 4, 8, and 15 K) as a function of magnetic field between 0 and 7 T. The resulting sets of VTVH-MCD curves are shown in Figure 6. By convention, the curves are plotted against $\beta H/2kT$ and the intensities are normalized.

The MCD theory for $S > 1/2$ systems was discussed in a recent paper by Neese and Solomon in which they derived a relationship between MCD *C*-term saturation behavior, transition polarizations, and spin Hamiltonian parameters.[28] Their expressions differ substantially from those employed previously by Werth et al. and Larrabee et al. to analyze the VT-MCD data of pseudo-tetrahedral Co(II) complexes.[5,18] In these earlier studies, the splitting between the two Kramers doublets, Δ, was estimated by measuring the intensities of the *C*-term and *B*-term contributions from each doublet at various temperatures. This method yields the value of Δ but fails to provide values for spin Hamiltonian and other parameters (*D*, *E/D*, *g* values, transition polarizations). In contrast, these parameters are readily obtained from VTVH-MCD fits using the software developed by Neese.[28]

The VTVH-MCD saturation behavior depends on eight such parameters: *D*, *E/D*, the three *g* values, and the three polarizations. As it is not feasible to fit the data by varying all parameters simultaneously, the four VTVH-MCD curves were first fit in the axial limit of $E/D = 0$, since previously published X-band EPR spectra of solid $CoCl_2(PPh_3)_2$ suggest a near-axial system.[13] The intrinsic *g* values were also estimated from the X-band EPR spectrum, which exhibits resonances at $g' \approx 4.6$ and 2.2, suggesting that $g_x \approx g_y \approx 2.3$ and $g_z \approx 2.2$. The value of *D* was then systematically varied with all of the other spin-Hamiltonian parameters held constant, and for each value of *D* the three polarizations were fit to achieve the best agreement between experimental and calculated VTVH-MCD data. The goodness of fit was judged from the χ^2 parameter, analogous to the method described above for HFEPR fits.

(41) Menzel, E. R.; Vincent, W. R.; Johnson, D. K.; Seebach, G. R.; Wasson, J. R. *Inorg. Chem.* **1974**, *13*, 2465−2473.
(42) Tomlinson, A. A. G.; Bellitto, C.; Piovesana, O. *J. Chem. Soc., Dalton Trans.* **1972**, 350−354.
(43) Coleman, J. E.; Coleman, R. V. *J. Biol. Chem.* **1972**, *247*, 4718−4728.
(44) Kato, H.; Akimoto, K. *J. Am. Chem. Soc.* **1974**, *96*, 1351−1357.

The 751 nm VTVH-MCD data set showed the greatest "nesting" (Figure 6), and the fit of this set was the most sensitive to the value of D and clearly favored large negative values for this parameter.[45] In contrast, for the remaining three data sets, which showed less nesting, the quality of the fits were less strongly dependent on D (see Figure S1 in Supporting Information). This result emphasizes the need to measure the saturation behavior of several peaks to obtain accurate spin Hamiltonian parameters from VTVH-MCD. To evaluate the effect of D on the overall goodness of fit, the χ^2 values for all four VTVH data sets were summed to produce a composite plot ($\Sigma\chi^2$), shown in Figure S3(a). The best fits were obtained for D values < -10 cm^{-1}, with a shallow global minimum at -15 cm^{-1}. On the basis of Figure S3(a), it is reasonable to conclude that D lies close to -15 cm^{-1}, although it is possible to state with confidence only that $D < -10$ cm^{-1}.

The fact that the $\Sigma\chi^2$ values remain fairly constant as D becomes increasingly negative is not surprising. As D grows larger in magnitude, the population of the higher Kramers doublet becomes virtually zero across the temperature range employed in the VTVH-MCD experiment (2−15 K). Further increases in $|D|$ then fail to change the overall shapes of the saturation curves.

Simulations for an $S = 3/2$ system with $D = -15$ cm^{-1} and $E/D = 0.10$ with various polarizations indicated that the overall shapes of the VTVH-MCD curves are not drastically affected by changes in the E/D ratio (data not shown). This is because the g' values of the $M_S = \pm 3/2$ doublet are relatively insensitive to changes in E/D, in contrast to the g' values of the $M_S = \pm 1/2$ doublet. Since for large negative D values only the $M_S = \pm 3/2$ doublet is significantly populated at $T < 15$ K, changes in E/D are not expected to result in major changes in saturation behavior. Nevertheless, it was possible to estimate the degree of rhombicity in $CoCl_2(PPh_3)_2$ by systematically fitting the four sets of VTVH-MCD curves over a range of fixed E/D ratios. As shown in Figure S3(b), the effect of variation in the E/D ratio is similar at three representative D values. The best global fit was obtained for $D = -12$ cm^{-1} with $E/D = 0.08$ and $g'_x = 4.8$. From these results we can safely conclude that $0.06 < E/D < 0.12$, with a slight preference for $E/D \approx 0.08$.

Finally, the real g_z parameter was adjusted at various D and E/D values to assess its effect on the VTVH-MCD fits. In general, a smaller g_z value in the range of 2.20−2.15 was preferred. Taking into account the ranges over which good fits are obtained, the MCD spin Hamiltonian parameters can be given as $D = -14(3)$ cm^{-1}, $E = 0.96(20)$ cm^{-1}, $g_x = 2.15(5)$, $g_y = 2.16(4)$, and $g_z = 2.17(3)$. The agreement between these parameters and the ones derived from HFEPR is remarkable, and it should be noted that the VTVH-MCD data were analyzed without any prior knowledge of the HFEPR results presented above.

Discussion

A dependable interpretation of conventional EPR spectra of high-spin Co(II) is difficult and has led to controversies as to their possible origin.[8,46] Apparently even very basic information such as the sign of zfs remains in many cases in doubt, since a definitive determination of this parameter usually requires high frequency and field conditions, as was done on single crystals.[20] We offer here an alternative to that method that does not require a single crystal but benefits from the torquing effect of a strong magnetic field on a polycrystalline sample. We also extend significantly the range of zfs available for experimental determination to 30 cm^{-1} and beyond through the use of novel sub-THz sources, backward wave oscillators.

We will start with comparing the results of HFEPR determination of zfs in $CoCl_2(PPh_3)_2$ with those from other techniques, including MCD data obtained here. Over the past 40 years, various magnetic measurements have been made on this complex.[16,47,48] These studies, even the most recent and detailed among them, that of Carlin et al.,[16] demonstrate a limitation of magnetic measurements in determining zfs. Carlin et al. could not determine the magnitude of zfs (it was considered to be relatively large), though specific heat data led them to propose the $\pm 3/2$ Kramers doublet as the lower-lying level,[16] that is, negative D, in agreement with our results.

Of greatest relevance is the comparison with the X-band EPR spectra (at 3.6 K) and CW EPR power saturation behavior of powder $Co_{0.002}Zn_{0.998}Cl_2(PPh_3)_2$ and of $CoCl_2(PPh_3)_2$ in ethanol frozen solution reported by Makinen et al.[13] The doped powder exhibits features at $g' \approx 4.6$ and 2.2 (Figure 2 of ref 13); g' values for the frozen solution were not given, although the spectrum resembles that of the doped powder (Figure 3 of ref 13).[49] Simulation of an X-band spectrum using the parameters determined by HFEPR for $CoCl_2(PPh_3)_2$ (using $\nu = 9.0-9.5$ GHz) affords the following effective $\mathbf{g}$ matrix: $\mathbf{g}' \approx$ [4.8, 3.8, 2.2] (the parameters determined independently by VTVH-MCD yield $\mathbf{g}' \approx$ [4.8, 3.8, and 2.1]). The component g' values are in good agreement with those reported by Makinen et al., given that the middle of these would not likely be resolved in their very broad X-band spectrum (Figure 2 of ref 13). The reverse, namely, extraction of zfs from the X-band EPR spectra, is very difficult. This procedure requires resolution of all three g' values ($\mathbf{g}' = [g_{x'}, g_{y'}, g_{z'}]$), combined with assumptions as to the intrinsic g values ($\mathbf{g} = [g_x, g_y, g_z]$), which then allows determination of $|E/D|$ (see eq 9 in Banci et al.;[3] much more elaborate formulas are given by Pilbrow[50]). The relation of these intrinsic g values to the electronic structure of transition-metal ions has been given by McGarvey.[14] His method allows extraction of D and E directly from the intrinsic g values, also requiring a value for the multielectron spin−orbit coupling constant, λ (see eq 77 in ref 14). However, this method ignores spin−orbit coupling from excited states with different spin multiplicity from the ground state; thus, "eq 77 is not appropriate for the case of d^3"[14] nor for d.[7] Taking as an example $CoCl_2(PPh_3)_2$, use of the free-ion value for $\lambda = -178$ cm^{-1},[24] likely an overestimate, and the intrinsic g values from HFEPR gives $D = -6.4$ cm^{-1}, $|E| = 0.18$ cm^{-1}, both much lower in magnitude than found experimentally. Clearly, even in cases of good resolution of g' values,

(45) The band at 751 nm exhibits many of the characteristics of MCD B-terms, although its intensity is weakly temperature-dependent. For M_{xz}- and M_{yz}-polarized transitions, the relevant molecular orientations are such that the y and x axes, respectively, are collinear with the external magnetic field.[28] In this case, the splitting of the $M_S = \pm 3/2$ doublet is proportional to the effective g_y and g_x values which are zero for axial systems with large D values. As a consequence, the only temperature dependence of the MCD signal arises from field-induced mixing between the $\pm 3/2$ and $\pm 1/2$ doublets of the $S = 3/2$ ground state. The VTVH-MCD fitting program used in this study accounts for this behavior.

(46) Jesson, J. P. *J. Chem. Phys.* **1968**, *48*, 161−168.
(47) Cotton, F. A.; Faut, O. D.; Goodgame, D. M. L.; Holm, R. H. *J. Am. Chem. Soc.* **1961**, *83*, 1780−1785.
(48) Davies, J. E.; Gerloch, M.; Phillips, D. J. *J. Chem. Soc., Dalton Trans.* **1979**, 1836−1842.
(49) The solution structure of $CoCl_2(PPh_3)_2$ likely differs from that in solid, as discussed by Makinen et al.[13] and corroborated by us, which will be reported separately.
(50) Pilbrow, J. R. *J. Magn. Reson.* **1978**, *31*, 479−490.

which is uncommon, conventional EPR alone is insufficient for determining zfs values and for allowing their subsequent interpretation.

Turning to the method of CW EPR power saturation, as described by Yim et al.,[51] a negative value of D results in an *apparent* value of zero for the zfs, which was evidently the case for doped powder $CoCl_2(PPh_3)_2$.[13] This inability to determine the magnitude of zfs when it has a negative sign is clearly a severe limitation of the EPR power saturation technique. However, there is no qualitative conflict between the original saturation studies[13] on one hand and our current HFEPR and MCD results on the other: all give $D < 0$ for $CoCl_2(PPh_3)_2$. An EPR line width measurement led Makinen et al. to estimate a zfs value of -6 cm^{-1} ($D \approx -3$ cm^{-1}),[13] a much smaller magnitude than that found by HFEPR or MCD. Furthermore, we note that pulsed versus CW X-band EPR spectra of a given high-spin Co(II) complex can exhibit very different spectral line shapes,[37] and the line shapes of 35 GHz spectra can be very sensitive to instrumental parameters.[52] We thus suggest that line width measurements in EPR spectra of Co(II) are unreliable for quantitative purposes, in particular estimation of zfs.

The final experimental comparison is between HFEPR and VTVH-MCD, where for the first time we have performed parallel studies on the same complex in the same state using these two techniques. The values for spin Hamiltonian parameters were obtained from analysis of the MCD data for $CoCl_2(PPh_3)_2$ at multiple wavelengths using the recently developed method of Neese and Solomon.[28] The two parameter sets are as follows: HFEPR: $D = -14.76(2)$ cm^{-1}, $E = 1.141(8)$ cm^{-1}, $g_x = 2.166(4)$, $g_y = 2.170(4)$, $g_z = 2.240(5)$; VTVH-MCD: $D = -14(3)$ cm^{-1}, $E = 0.96(20)$ cm^{-1}, $g_x = 2.15(5)$, $g_y = 2.16(4)$, and $g_z = 2.17(3)$. There is thus a remarkable agreement between the two sets of independently determined fit parameters. After concluding the separate analyses of the MCD and HFEPR data, the VTVH-MCD data were also fit with the spin Hamiltonian parameters determined by HFEPR. The resulting fit was not as good as that obtained with the optimized parameters directly from VTVH-MCD but was still acceptable. In particular, the D and E/D values from HFEPR are certainly compatible with the MCD data. It does appear that the VTVH-MCD curves require smaller intrinsic g values, especially for g_z. Indeed, the larger value of g_z from the HFEPR results is the primary reason the quality of the VTVH-MCD fit is not optimal. The reason for this discrepancy may lie in the fact that in HFEPR the g_z value was determined mainly from the parallel $|-3/2\rangle - |+3/2\rangle$ transition (the $g' \approx 6.6$ line), which is influenced by artifacts due to incomplete torquing; thus, its accurate position is difficult to specify. In any case, the greatest controversy and potentially the most structural and electronic information lies in the zfs parameters, not the g values. Hence, the general agreement between HFEPR and VTVH-MCD in the D and E/D values is paramount.

We can also touch on the meaning and/or utility of the zfs parameters. The zfs and optical spectra in the homoleptic complex, $[CoCl_4]^{2-}$, wherein the only variation is in the angular distortion of the chloro ligands,[53] have been well determined experimentally in the solid state[20,54] and fully explained by crystal/ligand field theory.[19,46] However, in heteroleptic (lower symmetry) complexes, which are more relevant to metalloprotein active sites, the situation concerning the experimental determination of D (sign and magnitude) is unclear. For example, the sign of D is neither readily predicted nor easily determined by X-band EPR, and this technique cannot conclusively provide the magnitude of D. Our results ($D < 0$) for $CoCl_2(PPh_3)_2$ (C_{2v} symmetry) agree with those of Guggenberger et al.,[55] who attributed the X-band EPR spectra of a complex having overall C_2 symmetry,[56] to transitions within the $\pm 3/2$ doublet rather than within the $\pm 1/2$ doublet, i.e., $D < 0$. However, X-band EPR spectra of $CoCl_2(OPPh_3)_2$ [8] (C_2 symmetry and generally very similar to $CoCl_2(PPh_3)_2$) were attributed to transitions within the $\pm 1/2$ doublet, $D > 0$. The current results are of even more importance since we were able to determine the complete zfs including the E term and accurate (intrinsic) g values, all of which might form the basis for detailed ligand-field calculations, such as those described by Larrabee et al.[18]

The very broad range of resonant magnetic fields and frequencies available with current HFEPR instrumentation makes this technique likely the most accurate and definitive method for determining spin Hamiltonian parameters in amenable model high-spin Co(II) complexes. Given its steady progress, HFEPR will possibly become suitable to studying Co-substituted enzymes in the future as well. However, the important conclusion from this study is that VTVH-MCD, which can be applied to dilute solutions,[40] with use of the latest analytical methodology,[28] yields results that are fully consistent with HFEPR in a case where both techniques can be applied side by side. Such reliably analyzed experimental data can in turn lead to a better understanding of high-spin Co(II) complexes on a case by case basis.

Acknowledgment. We thank Prof. Kurt Warncke, Emory University, for helpful discussions and Dr. Charles J. Walsby, Northwestern University, for describing unpublished work. This work was supported by NHMFL, Roosevelt University, and the University of Wisconsin. The Sloan Research Fellowship Program (T.C.B.) and the NSF Graduate Research Fellowship Program (A.T.F.) are also acknowledged. The 25 T resistive magnet was funded by the Keck Foundation.

Supporting Information Available: Three figures (S1−S3) illustrating the fits of spin Hamiltonian parameters to the experimental MCD data. This information is available free of charge via the Internet at http://pubs.acs.org. See any current masthead page for ordering information and Web access instructions.

JA039257Y

(51) Yim, M. B.; Kuo, L. C.; Makinen, M. W. *J. Magn. Reson.* **1982**, *46*, 247−256.
(52) Walsby, C. J.; Hoffman, B. M. Personal communication of unpublished results.
(53) $[CoCl_4]^{2-}$ as found in Cs_3CoCl_5 has D_{2d} symmetry and is slightly elongated, while $[CoCl_4]^{2-}$ in Cs_2CoCl_4 has nearly C_{2v} symmetry and is slightly compressed; the former has $D < 0$, and the latter has $D > 0$.
(54) Ferguson, J. *J. Chem. Phys.* **1963**, *39*, 116−128.
(55) Guggenberger, L. J.; Prewitt, C. T.; Meakin, P.; Trofimienko, S.; Jesson, J. P. *Inorg. Chem.* **1973**, *12*, 508−515.
(56) $[H_2B(pz)_2]_2Co$, where $H_2B(pz)_2$ is dihydrobis(1-pyrazolyl)borate; providing a N_4 donor set.